State-dependent linearisation of mixture representations by the olfactory bulb

Aliya Mari Adefuin, Janine Kristin Reinert, Sander Lindeman, Izumi Fukunaga

Sensory and Behavioural Neuroscience Unit, Okinawa Institute of Science and Technology Graduate University

Abstract

Sensory systems are often tasked to analyse complex signals from the environment, to separate relevant from irrelevant parts. This process of decomposing signals is challenging when component signals interfere with each other. For example, when a mixture of signals does not equal the sum of its parts, this leads to an unpredictable corruption of signal patterns, making the target recognition harder. In olfaction, nonlinear summation is prevalent at various stages of sensory processing, from stimulus transduction in the nasal epithelium to higher areas, including the olfactory bulb (OB) and the piriform cortex. Here, we investigate how the olfactory system deals with binary mixtures of odours, using two-photon imaging with several behavioural paradigms. Unlike previous studies using anaesthetised animals, we found the mixture summation to be substantially more linear when using awake, head-fixed mice performing an odour detection task. This linearisation was also observed in awake, untrained mice, in both engaged and disengaged states, revealing that the bulk of the difference in mixture summation is explained by the brain state. However, in the apical dendrites of M/T cells, mixture representation is dominated by sublinear summation. Altogether, our results demonstrate that the property of mixture representation in the primary olfactory area likely reflects state-dependent differences in sensory processing.

Introduction

As animals in nature navigate through their environment in order to find food, mates, and to avoid dangers, their sensory systems are tasked to detect and recognise signals of interest despite a background of interfering signals. This figure-ground segregation is a ubiquitous task for many, if not all, sensory systems. In the visual system, for example, segmentation of spatial pattens of light allows animals to recognise objects despite some parts being obscured (Marr, 2010). In the auditory system, spectral combinations of sound waves are recognized and strung together over time to form a stream, allowing animals to recognise social calls from specific individuals among other noises (Bregman, 1990). In olfaction, too, animals face challenges in identifying an odour of interest in the presence of other molecules (Laing and Francis, 1989; Rokni et al., 2014).

Olfactory stimuli are first detected by a large family of olfactory receptors residing in the nasal epithelium (Buck and Axel, 1991). Due to a broad ligand-receptor binding (del Mármol et al., 2021), each odour molecule may activate a number of olfactory receptor types, leading to combinatorial representations (Malnic et al., 1999). As a result, when several compounds are present in a given mixture, they can activate overlapping sets of olfactory receptors, causing complex pharmacological

interactions. For example, molecules may bind a common receptor, which, depending on the efficacy, can lead to antagonism (Cruz and Lowe, 2013; Kurahashi et al., 1994; Oka et al.; Reddy et al., 2018; Singh et al., 2019), or enhancement (Xu et al., 2020). Recent large-scale studies demonstrate that this is a widespread phenomenon (Inagaki et al., 2020; Xu et al., 2020; Zak et al., 2020), which means that neural responses to mixtures often do not equal the sums of responses to the individual odours. In addition to the interactions in the periphery, there are many forms of nonlinear summation at multiple stages of olfactory processing, including the saturation of neural responses (Firestein et al., 1993; Wachowiak and Cohen, 2001) and inhibitory interactions in the olfactory bulb (Economo et al., 2016). Widespread suppressive interactions are also observed in downstream areas, including the piriform cortex (Penker et al., 2020; Stettler and Axel, 2009).

Nonlinear summation of signals in some brain areas is desirable, for example, when specific combinations of signals carry special meanings (Agmon-Snir et al., 1998; Jacob et al., 2008). However, in primary sensory areas, it is sometimes considered information limiting (Laughlin, 1989). For olfaction, this is thought to limit the analytical ability – whether a mixture *can* be perceived in terms of the constituent qualities (Jinks and Laing, 1999). Nonlinear summations, or "interactions", do not occur for all odour mixtures (Fletcher, 2011; Gupta et al., 2015; Tabor et al., 2004), but occur prevalently when the background and target activation patterns overlap. This happens when a mixture contains many components (Mathis et al., 2016), as well as when the background odours are structurally related the target odour (Cruz and Lowe, 2013; Fletcher, 2011; Jinks and Laing, 1999; Kay et al., 2003; Mathis et al., 2016; Tabor et al., 2004). Nonlinear summation poses a difficulty because it may distort a pattern of interest brought by non-uniform addition of unpredictable background patterns. Thus, the difficulty of demixing olfactory perception of mixtures goes beyond the challenge of detecting signals above noise. Due to this difficulty, some studies have suggested that the olfactory system may not decompose mixture representations into component parts, but instead, solve the task by learning task-specific boundaries (Mathis et al., 2016; Wilson and Stevenson, 2003).

The question therefore remains: how does the mammalian olfactory system deal with nonlinear summation of responses? To investigate this, we used binary mixtures of odours to investigate mixture representations in mice performing tasks. While temporal structures caused by turbulence may be used to segregate odours of interest from the background (Ackels et al., 2021; Hopfield, 1991), we tackle the case when temporal information from the environment is not available. We demonstrate, by comparing the mixture responses using various paradigms, that the property of mixture summation depends on the brain state. Our results further suggest that the linearization is implemented in the olfactory bulb, emerging in the deeper layer.

Results

Olfactory figure ground segregation is most difficult when the target and background odours evoke overlapping activity patterns (Rokni et al., 2014). To study this task using binary mixtures, we first characterized how our target odour relates to other odours in our panel. The target odour was ethyl butyrate and the rest of the odours in our set comprised a range of small esters structurally similar to ethyl butyrate, as well as non-esters (Fig. 1A). According to Rokni et al., the masking index, which measures the amount of overlap in response patterns between the target odour and background odours, correlates well with behavioural performances (Rokni et al., 2014).

To measure the masking indices from single odour responses, we obtained activity patterns from the OB output neurons, the mitral and tufted (M/T) cells. Using a two-photon microscope, we imaged from the glomerular layer of the olfactory bulb in *Tbet-Cre::Ai95D* mice, which express the calcium indicator GCaMP6f (Dana et al., 2019) in M/T cells (Haddad et al., 2013). To reproduce previous results, these initial imaging experiments took place in mice under anaesthesia (Fig. 1B). We studied the degree of overlap between ethyl butyrate and other odour responses, by presenting single odours in a randomized order. An analysis of glomerular activity patterns revealed that methyl butyrate responses overlap the most with the ethyl butyrate response patterns, followed by closely related esters (Fig. 1C-E).

Previous studies from anaesthetised animals showed that neural responses to odour mixtures exhibit widespread nonlinear summation (Inagaki et al., 2020; Oka et al.; Reddy et al., 2018; Singh et al., 2019; Xu et al., 2020). In particular, suppressive interactions become dominant among large responses, due to the saturation effect (Mathis et al., 2016). This pattern is observed at many stages of olfactory processing, including in the olfactory bulb (Economo et al., 2016; Fletcher, 2011) and anterior piriform cortex (Penker et al., 2020), but it depends on the complexity of mixtures, as well as odorant choices (Fletcher, 2011; Gupta et al., 2015; Rokni and Murthy, 2014; Tabor et al., 2004). We therefore characterized the property of binary mixture summation using our odour set.

We first confirmed that our olfactometer is capable of presenting stable concentrations of odours for mixtures, leading to linear sums of ionization levels when two odours are mixed (Fig. 2A-C). Then, to assess how the OB output represents binary mixtures, we imaged the individual somata of mitral and tufted cells in *Tbet-cre::Ai95D* mice (Fig. 2D). A typical session consisted of about 40 trials, to minimise time-dependent effects. Single odours and their binary combinations were presented in a semi-random order. Since ethyl butyrate, methyl butyrate, and the mixture of these two odours are of particular importance in this study, these three trial types appeared every 10 trials (Fig. 2E; see methods). To assess how the mixture of ethyl butyrate and methyl butyrate is represented, the amplitudes of the mixture responses were compared against those of linear sums of single odour responses (Fig. 2F,G). As reported before, a large proportion of M/T cells exhibited nonlinear summation (39.0% of M/T cells showed a deviation from linearity greater than 2; 71/182 ROIs, 7 fields of view, 4 mice) with a large fraction showing sublinear summation (35.7%, 65/182 ROIs). A simple feed-forward network performed was used to test if decoding the presence of component odours is easier when inputs sum linearly (Supplementary Fig. 1). This demonstrate that nonlinear summation can be a hindrance for demixing. Together, our results confirm that nonlinear summation is prevalent for closely related odours even in binary mixtures.

Given that nonlinear summation is so widespread in the OB output, how well can mice analyse binary mixtures at the behavioural level, to accurately detect the presence of the target odour? To assess this, we used a Go/No-Go paradigm for head-fixed mice. The rewarded stimulus (S+ odour) contained ethyl butyrate, either as a single odour or as a component of a binary mixture (Fig 3A). To train mice on this task efficiently, after habituation, the head-fixed mice were first trained to discriminate ethyl butyrate against other single odours (Fig 3A). The mice learned to perform this task well, reaching an accuracy of 80% within 200 trials on average (Fig. 3 B,C; number of trials to reach 80% accuracy = 194.3 ± 21.9; n = 7 mice). Subsequently, these mice were trained to detect the presence of ethyl butyrate in binary mixtures (Fig. 3B,C). The mice performed the mixture task at a high accuracy from the beginning (90.2 ± 1.3 % of trials with correct responses in the first session; n = 7 mice). However, the mistakes they made were odour-specific, in that they tended to lick more indiscriminately on methyl butyrate-containing trials regardless of the presence of ethyl butyrate (Fig 3D,E; mean lick preference index for MB trials = 0.74 ± 0.04 vs. 0.93 for 5 other background odours, p = 0.0035, 1-way ANOVA; n = 7 mice). However, with training, the performance on methyl butyrate trials, too, became accurate, demonstrating that mice are able to improve the ability to accurately detect the target odour in binary mixtures even when the background odour is similar.

To understand why mice were able to acquire the binary mixture task so easily, we sought to analyse the mixture representations of OB output neurons in trained, behaving mice. We performed two-photon imaging of M/T cell somata in a separate group of *Tbet-Cre::Ai95D* mice that were awake and accurately performing the mixture task (Fig 4A). Surprisingly, in these mice, ethyl butyrate and methyl butyrate mixture responses largely matched linear sums of the component responses. Only 8% of ROIs (16/202; n = 13 imaging sessions, 6 mice) showed sublinear summation. On the other hand, when the same animals were later anaesthetized, sublinear summation increased substantially, with 46% of ROIs (47/103; n = 8 imaging sessions, 4 mice). Notably, the difference was apparent already in the early phase of the evoked responses (Fig. 4D-F). This result indicates that the property of mixture summation is state-dependent, and linearization is not imprinted permanently as a result of learning.

To what extent does task learning affect the mixture summation? Previous studies suggest that prior exposures and familiarity to odours can affect the ability to analyse odour mixtures (Grabska-Barwińska et al., 2017; Poupon et al., 2018). To address this, we assessed how ethyl butyrate and methyl butyrate mixtures are represented in naïve but awake, head-fixed mice. We took care to engage the mice as much as possible, since the level of motivation, with an accompanying change in the sniff patterns, affects the property of the olfactory system (Carey and Wachowiak, 2011; Jordan et al., 2018). To this end, we presented the same sets of odour stimuli, but instead of associating specific odours with reward, the water reward was delivered on randomly selected trials (Fig. 5A). In this scenario, mice often generated anticipatory licks, but without discriminating between trials with vs. without ethyl butyrate (Fig 5B,C; mean number of licks for EB vs. non-EB trials = 3.40 ± 0.64 vs. 3.41 ± 2.01; p = 0.97, paired t-test, n = 20 sessions, 6 mice). We then assessed the mixture responses of M/T cells in naïve, engaged mice (Fig. 5D,E). Surprisingly, the ethyl butyrate and methyl butyrate responses summed linearly. As with the trained mice, the largely linear summation was observed in the early phase of the responses (Fig. 5D,E). Furthermore, M/T responses are comparable in amplitudes between awake, naïve, and engaged mice and trained mice performing the task (Fig. 5F).

The similarity of mixture representations between naïve mice and the mice that learned to accurately analyse binary mixtures, was surprising. Since the behavioral context is a crucial determinant of how different groups of OB neurons are recruited (Carey and Wachowiak, 2011; Jordan et al., 2018; Wachowiak, 2011), we assessed if the level of behavioural engagement affected the property of mixture summation at all. To test this, we designed a behavioural paradigm to make head-fixed mice disengaged toward odour presentations. The paradigm involved delivering the water reward every trial, 15-20 seconds before the onset of odour (Fig. 6A). The level of disengagement was confirmed by slow inhalations taken by the mice during odour, unmodulated from the baseline pattern, especially compared to trained mice performing the mixture task or naïve mice undergoing random reward association (Fig. 6B). When the mixture response properties of M/T cells were analysed, however, the mixture summation was found to be largely similar to awake, engaged mice (Fig 6C,D). In addition, when a normalization model was used to remove the small saturation effects that persists, the residual nonlinearity was comparable across brain states (Supplementary Fig. 2), indicating that no further linearization of summation occurs with training or task engagement. Overall, these experiments suggest that wakefulness explains the bulk of the state-dependent linearization of binary mixture representation by the OB output, rather than the training or the level of engagement.

Finally, we sought to understand at what stage of olfactory processing the linearisation is implemented. Since sensory information processing in the OB involves different interneuron types in the superficial vs. deep layers, we studied the mixture responses of M/T cells in the apical dendrites vs. somata (Fig 7). We found that, unlike in the somata, mixture summation is predominantly sublinear in the apical dendrites, with 44.7% of ROIs showing sublinear summation in trained mice performing the target detection task (38/85 ROIs, 7 sessions, 7 mice). This is despite the fact that odour-evoked responses are generally dampened in awake mice compared to the anaesthetised case (Supplementary Fig. 3). It is possible that an extra mechanism operates at, or near, the soma. For example, we found that an apparent, odour-locked inhibition associated with complex response waveforms in wakefulness (Kato et al., 2012), is restricted to somata (Supplementary Fig. 3). Altogether, the subcellular specificity suggests that a mechanism exists in the primary olfactory area that linearises mixture summation, which is absent under anaesthesia.

Discussion

Segmentation and extraction of relevant information from mixtures of signals are important and perpetual tasks for sensory systems. Nonlinear summation of signals can pose a difficulty in demixing component signals faithfully. In this study, by imaging from the primary olfactory area of awake mice while they analyse olfactory binary mixtures, we demonstrate that the signal summation in the primary olfactory area of the mouse is state-dependent. Generally, mixture summation is subject to less saturation effect and as a result more linear in awake mice, irrespective of the behavioural engagement level.

We also observed that the property of mixture summation depends on the subcellular compartment of the output neurons. This gives rise to two hints about the underlying mechanism. First, this makes it likely that some of the linearisation is implemented in the olfactory bulb. That is, a mechanism seems to adjust the dynamic range of mitral and tufted responses to odours, so that mixture responses remain below the saturation level. Second, the appearance of this phenomenon at the soma suggests that a mechanism located in a deeper layer is involved. For example, perisomatic inhibition mediated by granule cells and axonless interneurons of the external plexiform layer (Burton, 2017; Shepherd, 2004) are more likely than that by juxtaglomerular inhibitory neurons. Some short axon cells that ramify their processes at the level of M/T cell lateral dendrites, on the other hand, are reported to contact granule cell dendrites (Eyre et al., 2008), thus may not be the direct source of perisomatic inhibition we observed. The EPL interneurons and granule cells both exhibit odour-locked responses (Miyamichi et al., 2013), and affect odour responses of M/T cells (Shani-Narkiss et al., 2020). Further, both types show state-dependent modulation (Kato et al., 2012; Kato et al., 2013). In addition to inhibitory mechanisms, the apparent reduction in response amplitudes could arise from an increase in the baseline firing rates of M/T cells. A higher baseline calcium signal could result in reduced change in fluorescence during odour responses. However, since a difference in baseline firing rates is expected to affect the apical dendrites, too, it is difficult to explain the subcellular specificity of our observation with this factor alone. Exactly what circuit mechanism underlies our observation, causally, will be an intriguing question for future investigations. Finally, it is of note that, since the mechanism here is dependent on the brain state, it is likely different from stimulus-dependent mechanisms, such as sensory adaptation described in the retina (Laughlin, 1989).

Perception of olfactory mixtures has long fascinated investigators. Mixtures of odours often have qualities that are different from those of the individual components. Accurate recognition of components is particularly hard for human subjects. For untrained subjects, olfactory mixtures that contain about 30 components tend to smell alike (Weiss et al., 2012). Even highly trained people like perfumers can only accurately identify individual components if unfamiliar mixtures contained no more than 5 components (Poupon et al., 2018). These demonstrate an ultimate limit in the analytical ability. In addition, in untrained human subjects and rodents alike, when the task is to look for a particular aroma in the mixture, the tendency is to falsely report the presence of the target odour even when the mixture does not contain it (Laing and Glemarec, 1992; Rokni et al., 2014). In all cases, an extensive training for specific odours can improve the ability to detect the target odour, as seen in the case for sommeliers who routinely analyse key components in wines, which can contain several-hundred component mixtures (Ilc et al., 2016). Thus, while mixture perception is highly context specific (Rokni and Murthy, 2014), training in specific odours seems to be key to improving on mixture

analysis. With more complex mixtures, linearization in the olfactory bulb may reach a limit, and also is unlikely to be the only mechanism that is used to solve the task. Elucidating what role the primary sensory areas plays is a crucial step towards a mechanistic understanding of complex sensory processing.

Acknowledgement

We would like to thank Yu-Pei Huang and OIST's Animal Resource Service staff for their dedicated assistance, the members of Andreas Schaefer's group and Kevin Franks' group for comments on earlier versions of the work, and Adam Mago, Xiaochen Fu, and Josefine Reuschenbach for comments on the manuscript. This work was supported by the OIST Graduate University.

Methods

Animals

All animal experiments have been approved by the OIST Graduate University's Animal Care and Use Committee (Protocol 2016-151 and 2020-310). Tbet-Cre (Haddad et al., 2013) and B6J.Cg-Gt(ROSA)26Sor$^{tm95.1(CAG-GCaMP6f)Hze}$/MwarJ, also known as Ai95D (Madisen et al., 2015), were originally obtained from Jackson Laboratory (stock numbers 024507 and 028865, respectively). Tbet-Cre::Ai95D mice were generated by crossing homozygous Tbet-Cre and Ai95D mice resulting in heterozygous animals used for imaging experiments. C57Bl6J mice were purchased from Japan CLEA (Shizuoka, Japan) and were acclimatized to the OIST facility for at least 1 week before they were used for experiments. All mice used in this study were adult male (8 – 11 weeks old at the time of surgery).

Olfactometry

A custom-made flow-dilution olfactometer was used to present odours. Briefly, custom Labview codes were used to control to control solenoid valves, and flow controller (C1005-4S2-2L-N2, FCON, Japan) was used to regulate the rate of air flow. A pair of normally closed solenoid valves was assigned per odorant and used to odorise the air. These solenoid valves were attached to a manifold, such that a set of 8 pairs had access to the common stream of air. To generate binary mixtures of odours while keeping concentrations stable, one odour from each manifold (lines A & B) was used. For single odour presentations, odour was mixed with air passed through an empty canister. The odorised air was directed towards the animal only when the solenoid valve closest to the animal (final valve) opened. Final valve was opened for a short time (0.1 s for experiments involving behavioural analysis only, and 0.5 s for all imaging experiments, to accommodate for slow respirations during anaesthesia), to avoid adaptation related to temporal filtering for high sniff frequencies associated with long odour pulses (Verhagen et al., 2007). Total air flow, which is a sum of odorised air and the dilution air, was approximately 2 L/min, which was matched by the air that normally flows towards the animal. Inter-trial interval was approximately 40 seconds to ensure that the flow controllers have stabilised before each odour presentation. All odorants were from Tokyo Chemical Industry (Tokyo, Japan), apart for ethyl butyrate (W242705), which was from Sigma-Aldrich. Product number were: T0247 (Ethyl tiglate), V0005 (Methyl valerate), A0061 (Acetophenone), A0500 (Methyl anthranilate), B0757 (Butyl butyrate), B0763 (Methyl butyrate), S0015 (Methyl salicylate), S0004 (Salicylaldehyde), T0248 (Methyl tiglate), A0232 (Eugenol). Purity of all odorants was at least 98 % at the time of purchase. Stock odorants were stored at room temperature in a cabinet filled with N_2 and away from light.

Surgery

Head plate implantation: All recovery surgery was conducted in an aseptic condition. 8-11week old male C57Bl6/J mice were deeply anaesthetised with isoflurane. The body temprature was kept at 36.5 °C using a heating blanket with a DC controller (FHC, Bowdoin, USA). To attach a custom head plate about 1 cm in width weighing a few grams, the skin over the parietal bones was excised and the soft tissue underneath was cleaned, exposing the skull. The exposed skull was gently scarred with a dental drill, cleaned, dried, and coated with cyanoacrylate (Histoacryl, B.Braun, Hessen, Germany) before placing the headplate and fixing with dental cement (Kulzer, Hanau, Germany). For optical window implantation, adult, male *Tbet-Cre::Ai95D* mice were deeply anaesthetised, and underwent a window implantation procedure as previously described (Koldaeva et al., 2019). Briefly, after exposing

the frontal bone, a craniotomy about 1 mm in diameter was made over the left olfactory bulb and on the exposed dorsal surface, a cut piece of coverslip that snugly fit in the craniotomy, on the edge of the drilled bone, was gently pressed down and sealed with a cyanoacrylate and fixed with dental cement. Mice were recovered in a warm chamber, returned to their cages and given carprofen subcutaneously (5 mg/kg) for 3 consecutive days.

Habituation and behavioural measurements

Two weeks after surgery, water restriction started, and mice went through 3 days of habituation to head fixation, one session per day for approximately 30 minutes, until mice learned to lick vigorously for water reward. Respiration pattern was measured by sensing the air flow just outside the right nostril by placing a flow sensor (AWM3100V, Honeywell, North Carolina, USA), and the data was acquired at 1 kHz. Licking response was measured using an IR beam sensor (PM-F25, Panasonic, Osaka, Japan) that was part of the water port. Nasal flow, an analog signal indicating the odours used, lick signal, a copy of the final valve and water valve timing were acquired using a data acquisition interface (Power1401, CED, Cambridge, UK).

Discrimination training

After habituation, the head-fixed mice were trained to associate a water reward with a rewarded odour. The reward was two droplets of water (10 μl each), that arrived 3 seconds after the onset of the final valve opening. The mice underwent single odour discrimination training first, until they generated anticipatory licks in response to ethyl butyrate presentations, and correctly refrained from licking in response to other single odours. Once the overall accuracy was above 80% in at least one behavioural session, the mice went through the mixture detection task. A typical training session comprised roughly 100 trials, lasting about 1 hour. Rewarded trials comprised a third of all trials. Two-photon imaging took place once the mice performed at 80% accuracy or above.

Random association paradigm

After habituation, the head-fixed mice were presented with the same odour mixture stimuli as those that underwent the discrimination training. The water reward was delivered on randomly selected trials, 3 seconds after the onset of the final valve opening. One behavioural session was used to accustom the mice to the odours. Two-photon imaging commenced from the second behavioural session.

Disengagement paradigm

After habituation, the head-fixed mice were presented with the same odour mixture stimuli as above. The water reward was delivered every trial, 20 seconds before the onset of the final valve opening, arriving in the middle of the inter-trial interval, which was 40 seconds to ensure thorough purging to clear the lines, as well as to stabilize the flow controllers. Two-photon imaging commenced from the second behavioural session.

Odour mixture trial composition

Binary mixtures have been chosen due to the smaller number of possible odour combinations compared to more complex mixtures. However, even with 11 odours, there is a limit in the number of trials each head-fixed mouse can sample in a given session. We therefore decided to focus on the EB + MB mixtures. However, it was crucial that, EB, MB, and EB + MB mixture are not presented too

frequently, to avoid possible adaptation, as well as mice becoming over familiar, especially in the EB-detection task, where the goal was not to train mice to remember specific odour combinations. Thus, we used a compromise paradigm where EB, MB, and EB + MB appeared every 10 trials.

Data analysis

The data was anlaysed offline using custom Matlab codes. To calculate the accuracy, the number of licks during 3 seconds from the final valve onset was measured for each trial. Threshold for an anticipatory lick was set to 2, thus the correct response for rewarded trials was 2 or more beam breaks, and the correct response for unrewarded trials was 1 lick or less during the response time window. To calculate the learning curve, the accuracy was expressed as the proportion of correct trials in a given block of 50 trials. *Time to inhalation peak*: to calculate the speed of inhalation, onset of inhalation and peak of inhalation was detected using Spike2 (CED, Cambridge, UK), using the built-in event detection functions. Briefly, inhalation peaks were detected using the "rising peak" function. These events were used to search backwards in time for the inhalation onset, when the flow signal crossed a threshold value. *Lick preference index*: To measure how well mice discriminated rewarded vs. unrewarded mixtures, anticipatory licking patterns for the two types of trials were compared using the following formula:

$$\text{Lick preference index} = (\text{Lick}_{\text{rewarded}} - \text{Lick}_{\text{unrewarded}})/(\text{Lick}_{\text{rewarded}} + \text{Lick}_{\text{unrewarded}})$$

Where $\text{Lick}_{\text{rewarded}}$ corresponds to the average number of anticipatory licks on rewarded trials, and $\text{Lick}_{\text{unrewarded}}$ corresponds to that for unrewarded trials.

Imaging

A custom-made two-photon microscope (INSS, UK) with a resonant scanner was used to observe fluorescence from the olfactory bulb of *Tbet-Cre::Ai95D* mice *in vivo*. 3D co-ordinates for imaged field of view was recorded relative to the location of a reference, blood vessel pattern on the surface. Imaging from somata was done relatively superficially, just below the glomeruli, thus mainly comprised TCs, which use firing rate modulation to represent odours (Fukunaga et al., 2012). Fields of view for glomerular and somatic levels were 512 μm x 512 μm, and 256 μm x 256 μm, respectively, and overlapped for awake and anaesthetised conditions, but fewer sessions took place under anaesthesia. In each trial, 400 image frames were acquired at 30 frames per second, with 200 frames before the final valve opening to obtain steady baseline. Unless otherwise stated, the time window analysed for the odour-evoked responses was the first 1 second since the onset of final valve opening. For imaging under ketamine/xylazine anaesthesia (100 $mg.kg^{-1}$/20 $mg.kg^{-1}$ intraperitoneally), mice were kept on a warm blanket (FHC, Bowdoin, USA) to maintain the body temperature at 36 °C.

Image analysis

Transients were extracted as follows. Regions of interest (ROI) were manually delineated using an average frame from each imaging session. Pixel values within each ROI were averaged to obtain a time series. Imaging sessions with motion artefacts and drifts were removed from analyses. For each transient, the baseline period was defined as 2 seconds preceding the final valve opening. Relative fluorescence change ($\Delta F/F$) was calculated with respect to this baseline. Odour response period was 1 second (30 frames) starting at the onset of the final valve opening, unless otherwise stated. Awake mice tended to adjust sniff patterns, so the final valve opening was not triggered by nasal flow.

Masking index for the glomerular level was calculated as previously described (Rokni et al., 2014). Briefly, responses to single odours were obtained from glomeruli of anaesthetised mice. In each field of view, only the glomeruli responsive to the target odour (EB) were analysed. To obtain glomeruli evoked by the target odour, the evoked response amplitudes were converted into z-scores. Glomeruli that responded to ethyl butyrate with z-scores higher than 2 were considered. The masking index was the average overlap in the evoked response, where the maximum value for each glomerulus was 1. For each odour, responses were averaged over 3 or more trials. Mean and standard error of the mean are shown in figures, unless otherwise stated. Boxplots were constructed using the Matlab function *boxplot*, and show the median, 25th and 75th percentiles, and extreme data points not considered outliers. Outliers are shown with red crosses.

Deviation from linearity was the normalised difference between an observed mixture response amplitude and a linear sum of components:

Deviation from linearity = $(R_{observed} - R_{linear\ sum})/(s.e.m._{observed} + s.e.m._{linearsum})$

Where $R_{observed}$ is the mean response amplitude for observed mixture (e.g., response to EB + MB mixture), $R_{linear\ sum}$ is the trial average linear sum of component responses (e.g., EB response + MB response), and s.e.m. is the standard error of the mean for the corresponding amplitudes.

Decoding analysis

The decoding analysis was used to assess if nonlinear summation poses any difficulty for demixing, compared to linearly summed signals. The effect of nonlinear summation on decoding ability was assessed for M/T cells somatic responses from anaesthetised mice, presented with odour stimuli used in the mixture detection task (Supplementary Fig. 1). A simple feed-forward network with 1 hidden layer and three output units was trained using patternnet in Matlab. The input was single odour responses from each field of view. The hidden and output layers each received a weighted combination of the patterns from the previous layer. The output was trained to be 100, 010, or 001, for EB, MB, and other single odours, respectively. Due to the limited number of trials, the number of units in the hidden layer was 10. Cross validation was implemented by removing one trial each of responses to single EB and MB from the training set and assessing the performance of the trained network. To test how well the network performs for EB + MB mixture responses, the observed EB + MB responses from individual trials were fed into the trained network, and the output was averaged (3 or more trials per field of view). To generate a linear sum of EB + MB responses, the single EB and MB responses that had been removed from the training set were summed linearly and fed into the trained network.

Normalisation model

Previous studies observed that the saturation effect of mixture summation can be modelled by a normalization model (Mathis et al., 2016; Penker et al., 2020). The equation of normalization (Penker et al., 2020) was:

$$R_j^* = R_{max}\left(\frac{2}{1+e^{-s.R_j}} - 1\right)$$

where R_j represents the linear-sum amplitude of the jth neuron, R_j^* is the normalized response amplitude of jth neuron. Parameters s and R_{max} were obtained by fitting the data to observed mixture responses.

Figures

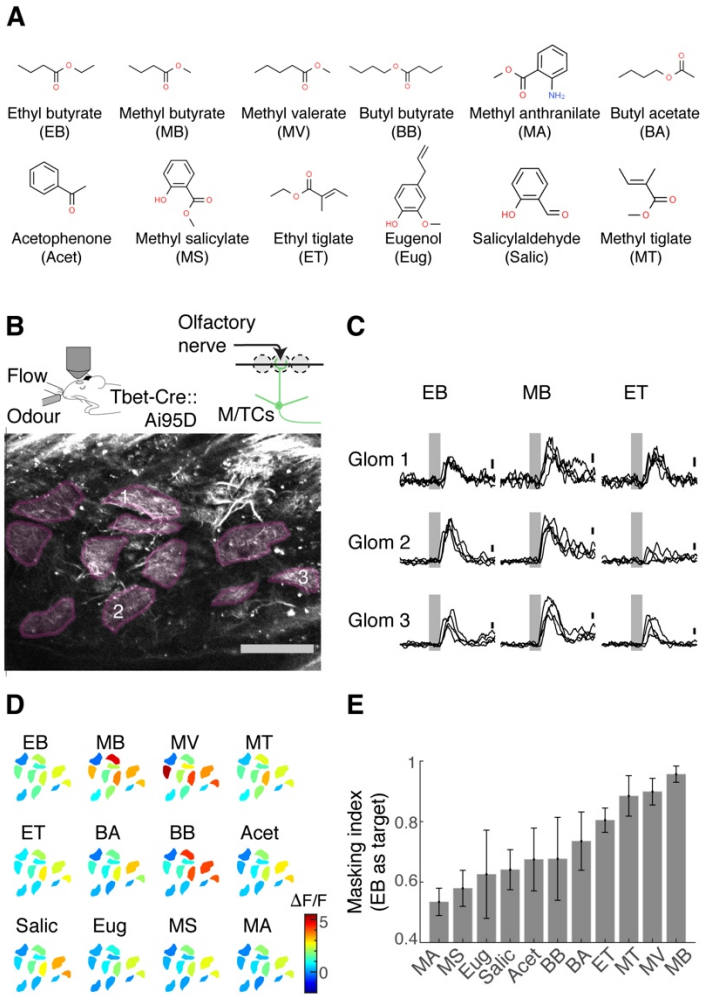

Figure 1: *Masking indices of odours used with respect to the ethyl butyrate pattern*

(**A**) Odours in the panel with abbreviations used in the rest of the manuscript. Ethyl butyrate was the target odour for behavioural experiments. (**B**) Two-photon imaging of GCaMP6f signals from the apical dendrites of M/T cells in *Tbet-Cre::Ai95D* mice under ketamine and xylazine anaesthesia. Scale bar = 0.1 mm. (**C**) Example GCaMP6f transients expressed as a change in fluorescence (ΔF/F). Scale bar = 1 ΔF/F. Gray = Odour presentation (0.5 s). (**D**) Example of evoked responses. Manually delineated ROIs are shown with fluorescence change evoked by odours, indicated with the corresponding colour map. The amplitude indicated is the average change during 1 second from the final valve opening. (**E**) Masking indices for all odours in the panel, with EB as the target. N = 4 fields of view, 4 mice. Mean and s.e.m. of 3 trials or more shown.

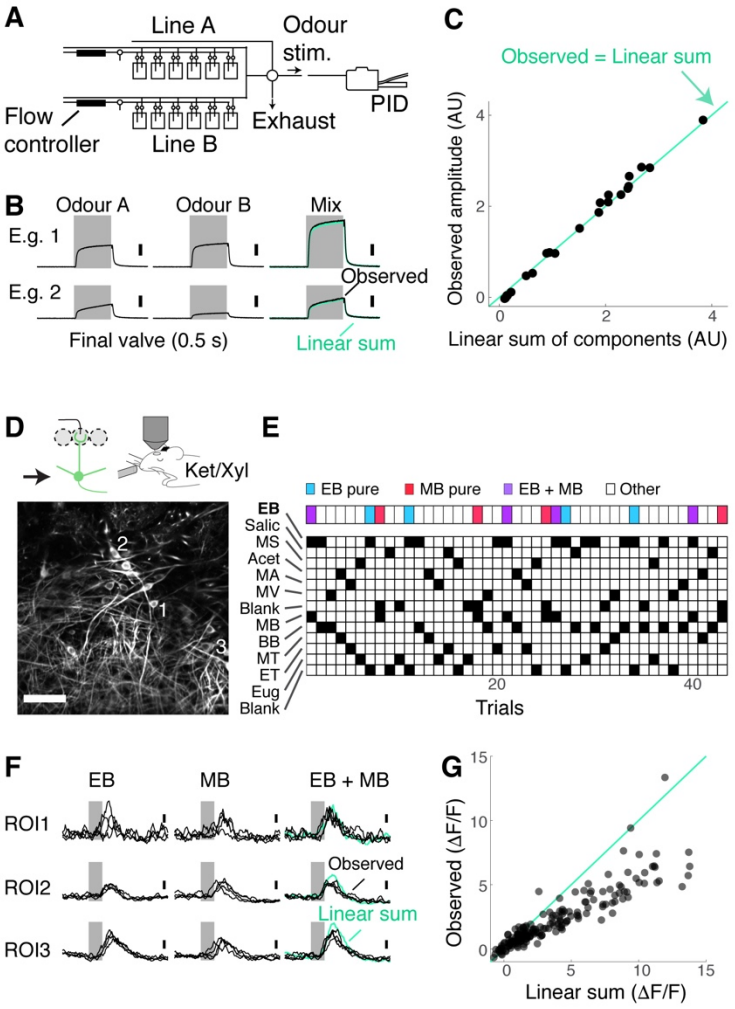

Figure 2: *Mixture suppression dominates under anaesthesia*

(**A-C**) *Validation of linear mixing by the olfactometer.* (**A**) Binary mixtures are generated by mixing odorized air from two streams each equipped with a mass flow controller and presented as a stimulus when a five-way valve ("final valve") is actuated. To present single odours, odorized air from one line was mixed with air that passes through a blank canister in the other line. A photoionization detector (PID) was used for calibration. (**B**) Example PID measurements for single odours ("Odour A" and "Odour B"), and their mixtures. Linear sum of the components (light blue trace) is shown superimposed with the observed PID signal (black). (**C**) Observed amplitudes for mixtures vs. linear sum of component amplitudes. Light blue line = the observed mixture amplitude equals the linear sum of components. (**D-G**) *Investigation of mixture summation by M/T cells under anaesthesia*. (**D**) Top: schematic, Two-photon GCaMP6f imaging from somata of M/T cells in naïve *Tbet-Cre::Ai95D* mice under ketamine/xylazine anaesthesia. Bottom: example field of view. Scale bar = 50 μm. (**E**) Example session structure. Single EB and MB trials, as well as EB+MB mixture trials, are indicated with colour codes. (**F**) Transients from 3 example ROIs. Linear sum (blue trace) was constructed by linearly summing averages of single EB and MB responses. Gray bar represents time of odour presentation (0.5 s). (**G**) Scatter plot of observed mixture response amplitude against linear sum of components. N = 183 ROIs, 7 fields of view, 4 mice.

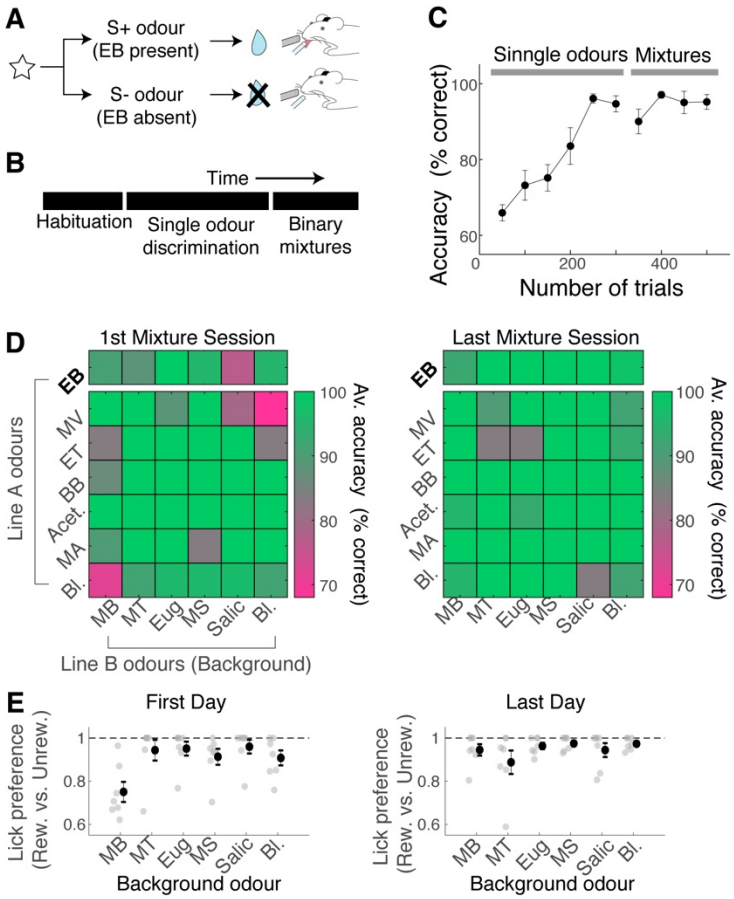

Figure 3: *Mice can learn to accurately analyse difficult binary mixtures*
(**A**) Behavioural paradigm: Go/No-Go task with head-fixed mice. EB-containing olfactory stimulus was the rewarded stimulus. (**B**) After habituation, mice learned to discriminate ethyl butyrate against other single odours in the panel. Once proficient, mice learned to detect the presence of ethyl butyrate in binary mixtures. 30% of stimuli in the mixture stage were single odours. (**C**) Behavioural performance for all mice (n = 7 mice). Mean and s.e.m. shown. (**D**) Odour-specific accuracy shown for the 1st (left) and last day of mixture training (right). Green shades indicate high accuracy. Top row corresponds to rewarded trials, and bottom 6 rows correspond to unrewarded trials. Average accuracy from all animals shown (n = 7 mice). (**E**) Lick preference index measures licks that occur preferenrially on rewarded trials for a given background odour. Relative lick of 1 occurs when all anticipatory licks were observed in rewarded trials. Gray points = data from individual animals; mean and s.e.m. shown in black.

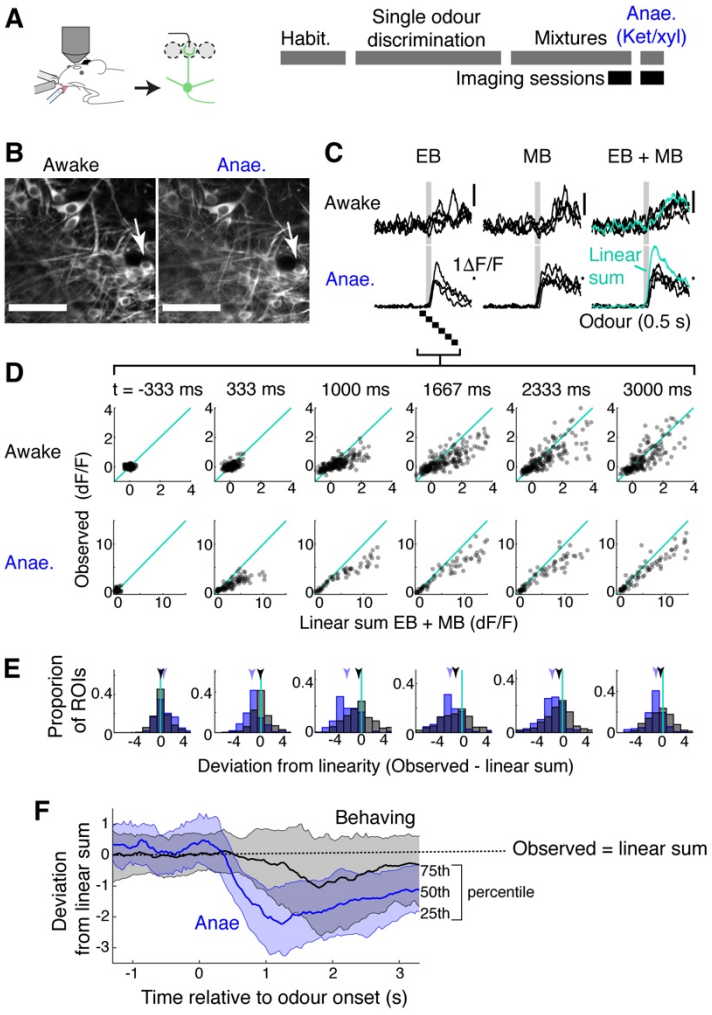

Figure 4: *Mixture summation is more linear in awake, behaving mice.*

(**A**) Schematic of experimental setup. Imaging of GCaMP6f signals from the somata in Tbet-Cre::Ai95D mice performing the mixture detection task. On the last day, imaging took place under ketamine/xylazine annaesthesia (Anae). (**B**) Example field of view showing the same neuron from two imaging sessions. (**C**) Relative fluorescence change evoked by EB, MB and their mixture for the two conditions, for the neuron indicated by arrow in (**B**). (**D**) Scatter plot of observed EB + MB mixture response amplitude against linear sum of component odour responses (average of 20 frames). Indicated time is relative to odour onset. (**E**) Summary of deviations from linearity, for data from trained, behaving mice (black) anaestherised mice (blue). (**F**) Timecourse of deviation from linearity. Central thick line is the median, and 25th and 75th percentiles shown below and above, respectively. N = 202 ROIs, 6 mice for behaving; 103 ROIs, 4 mice for anaesthetised case.

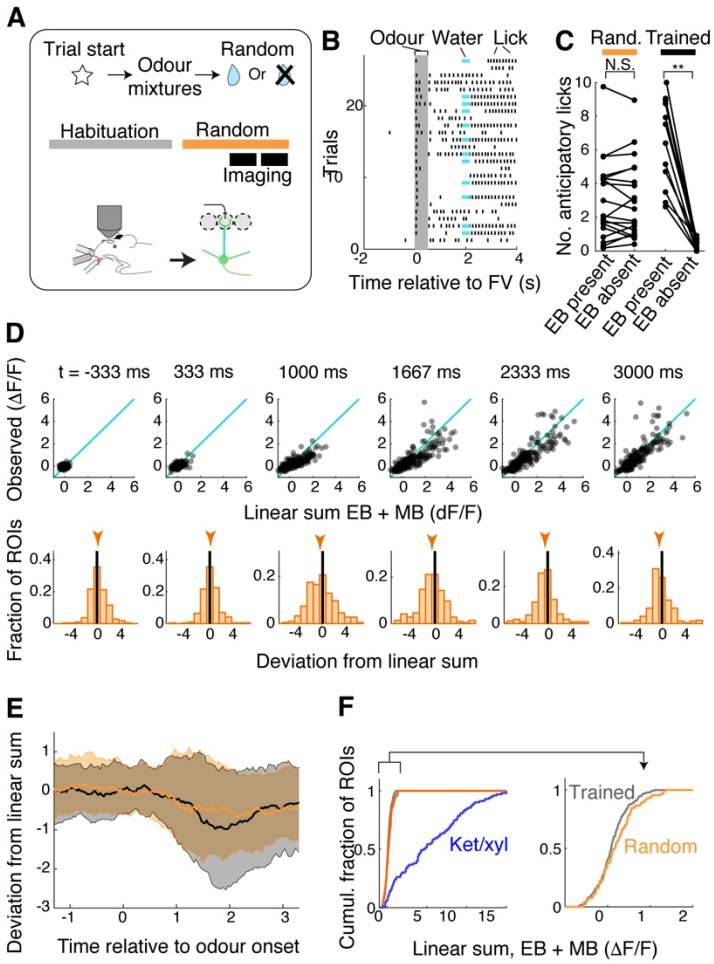

Figure 5: *Mixture summation is also largely linear in naïve, engaged mice*

(A) Schematic of experimental setup. **(B)** Lick raster from an example session relative to the final valve opening. Water reward delivery (2 seconds after the final valve onset) is marked with a pale blue line. Odour was presented for 0.5 seconds (gray). (**C**) Occurrence of anticipatory licks in EB-containing trials vs. trials where EB was not present, for random association sessions (left, "Rand."), shown next to the anticipatory lick patterns observed in mice trained to perform EB detection task (right, "Trained"). (**D**) Scatter plot of observed EB + MB mixture response amplitude against linear sum of component odour responses. Indicated time is relative to odour onset. (**E**) Summary of deviations from linearity as z scores, for data from trained, behaving mice (black) and mice that underwent random association (orange). (**F**) Left: Cumulative histogram of response amplitudes for linearly summed EB and MB, for ketamine/xylazine condition (blue), trained, behaving (gray) and random association (orange) cases. Right: Same as left panel, but with x-axis zoomed in as indicated. P = 0.19, two-sample K-S test.

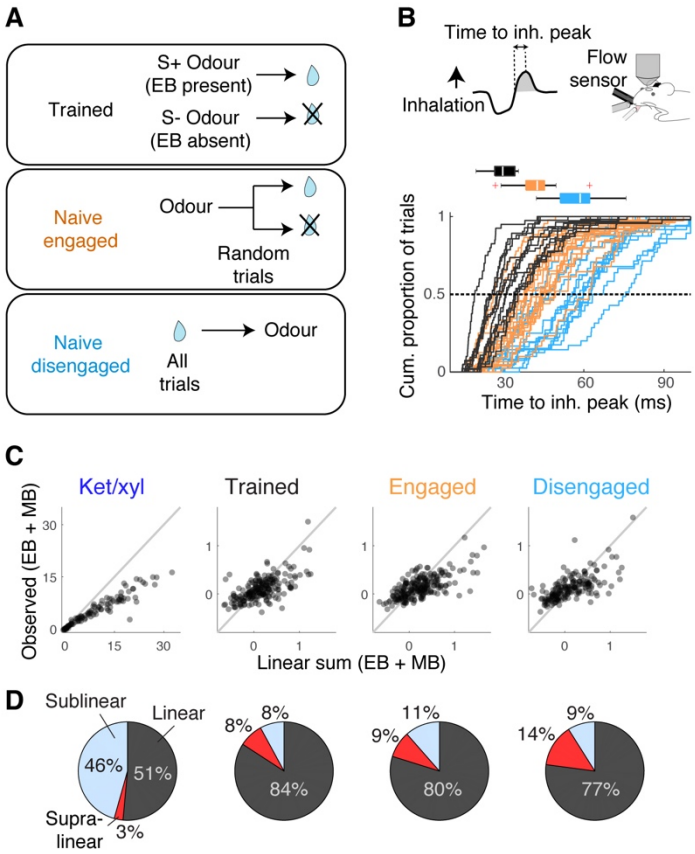

Figure 6: *Analyses under three behavioural paradigms demonstrate that wakefulness explains the bulk of linearisation*

(**A**) Contingency between odour and water reward for three behavioural conditions examined. (**B**) Analysis of inhalation speed to confirm the behavioural states; (top) time to inhalation peak was from the onset of inhalation to its peak, measured using a flow sensor. (bottom) Cumulative histogram of inhalation peak time during odour presentation, colour-coded by the paradigm (same colour code as panel **A**). Each line corresponds to each imaging session. Boxplots above describe the medians. (**C**) Side-by-side comparison of observed vs. linear sum of EB + MB response amplitudes for the conditions indicated. (**D**) Summary showing the proportion of ROIs showing sublinear (deviation < -2), supralinear (deviation > 2), or linear summation for the EB + MB mixture.

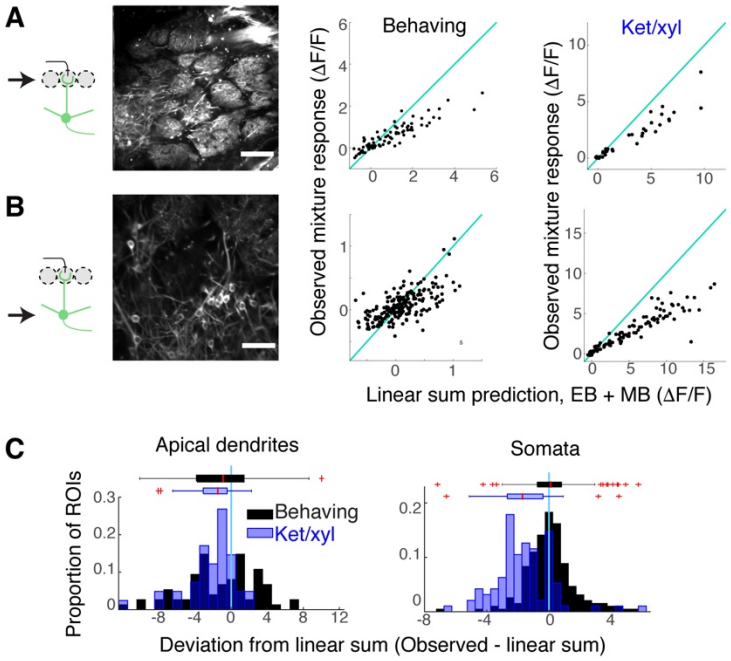

Figure 7: *Subcellular difference in mixture representation in trained, behaving mice*

(**A**) Left, example field of view showing GCaMP6f signals in *Tbet-Cre::Ai95D* mice, at the level of apical dendrites. Scale bar = 100 μm. Right, Scatter plots of observed EB + MB mixture responses against linear sum of single odour responses. Cyan line indicates the unity line, where summation is exactly linear. (**B**) Same as in **A**, but for individual somata, with scale bar = 50 μm. (**C**) Summary histograms showing deviation from linear summation (observed response amplitude – linear sum of component responses), expressed as the z-score.

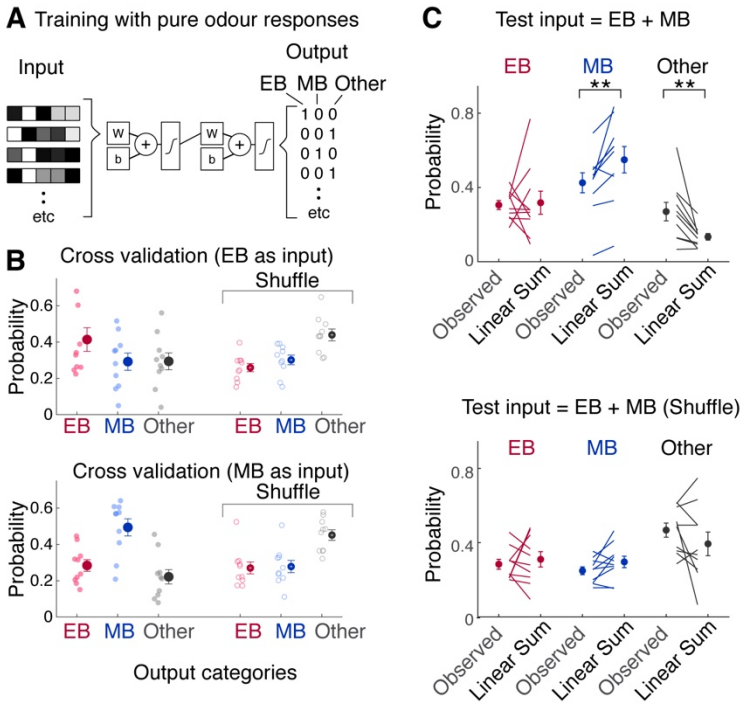

Supplementary figure 1: *Nonlinear summation adds difficulty to component pattern recognition*

(**A**) Schematic of the analysis. A simple, feed-forward network with 1 hidden layer (n = 10 nodes) was trained using activity patterns evoked by single odours. The output was a vector of 3 components, with 0 and 1 indicating the absence and presence of odour in the stimulus, respectively (EB, MB, and other odours). W = weights, b = bias. We chose not to test the binary classifier, because, mixtures containing the target and non-target odour will have multiple solutions (i.e., classification into target odour, and classification into non-target odour, are both correct). (**B**) Cross validation of the trained network. Response pattern to single odours not used for training was used as inputs. Network output when EB pattern was used as input (top), and when MB pattern was used as input (bottom). Shuffle control was obtained by randomly permutating the trial order. A better performance for decoding MB is likely a reflection of sensory tuning in the fields of view, as other decoders such as SVM gave similar results (data not shown). (**C**) Output of the network when input was the activity pattern evoked by EB + MB. To construct the linear sum of EB + MB responses (Linear Sum), one EB trial and one MB trial were removed from the training set. Their linear sum was used as the input pattern. The decoder classified the input into "other" odours more frequently when observed mixture responses were the inputs, compared to when the linear sum of component responses was used. p = 0.92 for EB, 0.0098 for MB, and 0.004 for other odours; Wilcoxson signed rank test; N = 13 fields of view from 6 naïve, anaesthetised mice.

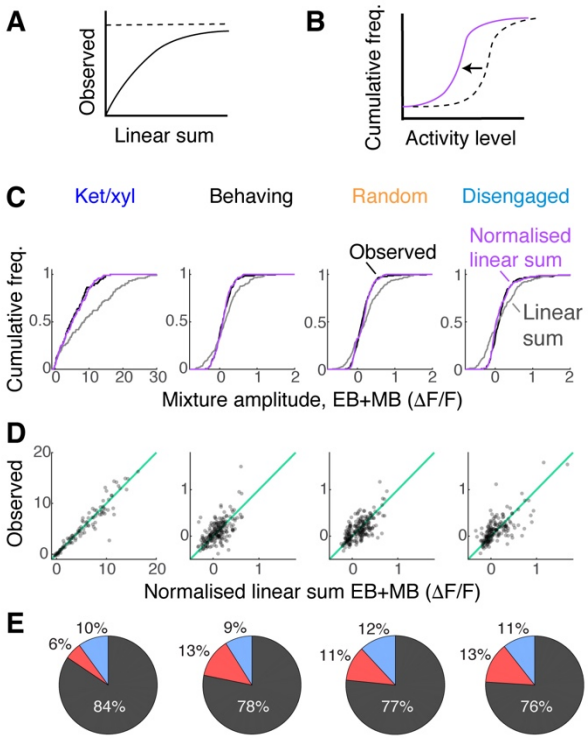

Supplementary figure 2: *No difference in residual nonlinear summation after normalisation*

(**A**) Neural responses are often normalized due to saturation of cellular mechanisms as well as actions by local inhibitory circuits. (**B**) Amplitude-dependent, saturation effect was removed by fitting the data using a standard normalisation model (Penker et al., 2020). Consequently, amplitude distributions of normalized linear sums were similar to those of observed EB + MB mixtures. (**C**) Cumulative histograms of response amplitudes, for linear sum (grey), Normalised linear sum (purple), and observed EB + MB responses (black). Distributions for normalised linear sum and observed responses should overlap perfectly when normalization is successful. (**D**) Relationship between the observed response and normalized linear sum for all conditions. (**E**) Proportions of ROIs showing sublinear summation (blue), supralinear summation (red), and linear summation (dark grey) after normalization, for the conditions indicated above.

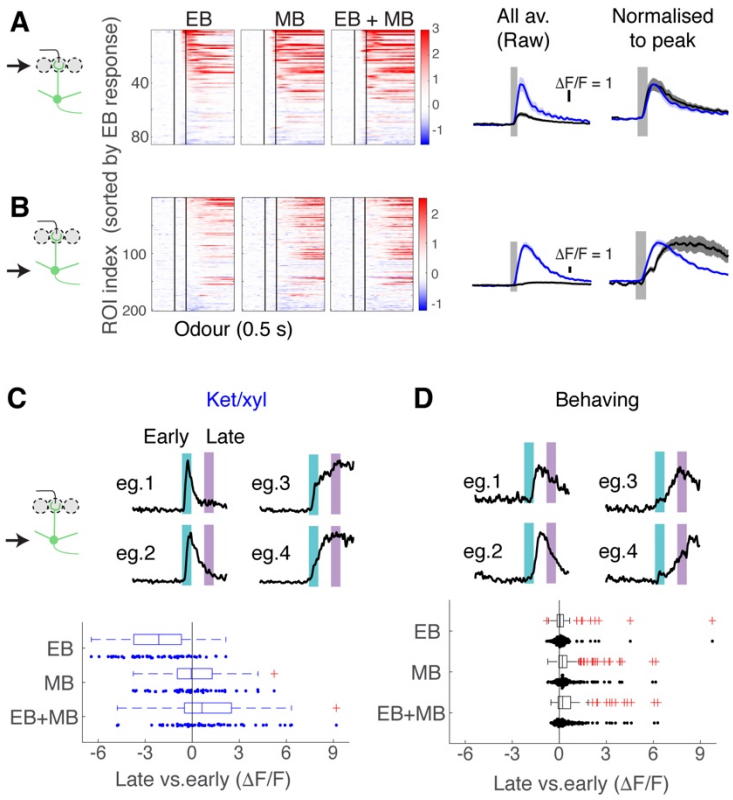

Supplementary figure 3: *Subcellular difference in the state-dependent temporal profile*

(**A**) Left: Evoked responses imaged from M/T cell apical dendrites of behaving mice, shown with the indicated colormap. Each ROI corresponded to a glomerulus. Right: Relative fluorescence change were averaged for all ROIs from behaving mice (black) and anaesthetised mice (blue), and shown as raw average, or when traces were normalized to the peak and averaged. Mean +- s.e.m. shown. (**B**) Same as in (A) but for M/T cell somata. (**C**) Quantification of the timecourse of evoked response in M/T cells somata of anaesthetised mice, expressed as the amplitude during late phase (purple) – amplitude during early phase (turquoise). Negative values indicate that early responses were larger. (**D**) same as (**C**), but for behaving mice.

References

Ackels, T., Erskine, A., Dasgupta, D., Marin, A.C., Warner, T.P.A., Tootoonian, S., Fukunaga, I., Harris, J.J., and Schaefer, A.T. (2021). Fast odour dynamics are encoded in the olfactory system and guide behaviour. Nature *593*, 558-563.

Agmon-Snir, H., Carr, C.E., and Rinzel, J. (1998). The role of dendrites in auditory coincidence detection. Nature *393*, 268-272.

Bregman, A.S. (1990). Auditory Scene Analysis: The Perceptual Organization of Sound (The MIT Press).

Buck, L., and Axel, R. (1991). A novel multigene family may encode odorant receptors: A molecular basis for odor recognition. Cell *65*, 175-187.

Burton, S.D. (2017). Inhibitory circuits of the mammalian main olfactory bulb. Journal of Neurophysiology *118*, 2034-2051.

Carey, R.M., and Wachowiak, M. (2011). Effect of Sniffing on the Temporal Structure of Mitral/Tufted Cell Output from the Olfactory Bulb. The Journal of Neuroscience *31*, 10615.

Cruz, G., and Lowe, G. (2013). Neural coding of binary mixtures in a structurally related odorant pair. Scientific Reports *3*, 1220.

Dana, H., Sun, Y., Mohar, B., Hulse, B.K., Kerlin, A.M., Hasseman, J.P., Tsegaye, G., Tsang, A., Wong, A., Patel, R.*, et al.* (2019). High-performance calcium sensors for imaging activity in neuronal populations and microcompartments. Nature Methods *16*, 649-657.

del Mármol, J., Yedlin, M.A., and Ruta, V. (2021). The structural basis of odorant recognition in insect olfactory receptors. Nature *597*, 126-131.

Economo, M.N., Hansen, K.R., and Wachowiak, M. (2016). Control of Mitral/Tufted Cell Output by Selective Inhibition among Olfactory Bulb Glomeruli. Neuron *91*, 397-411.

Eyre, M.D., Antal, M., and Nusser, Z. (2008). Distinct Deep Short-Axon Cell Subtypes of the Main Olfactory Bulb Provide Novel Intrabulbar and Extrabulbar GABAergic Connections. The Journal of Neuroscience *28*, 8217.

Firestein, S., Picco, C., and Menini, A. (1993). The relation between stimulus and response in olfactory receptor cells of the tiger salamander. The Journal of Physiology *468*, 1-10.

Fletcher, M.L. (2011). Analytical Processing of Binary Mixture Information by Olfactory Bulb Glomeruli. PLOS ONE *6*, e29360.

Fukunaga, I., Berning, M., Kollo, M., Schmaltz, A., and Schaefer, Andreas T. (2012). Two Distinct Channels of Olfactory Bulb Output. Neuron *75*, 320-329.

Grabska-Barwińska, A., Barthelmé, S., Beck, J., Mainen, Z.F., Pouget, A., and Latham, P.E. (2017). A probabilistic approach to demixing odors. Nature Neuroscience *20*, 98-106.

Gupta, P., Albeanu, D.F., and Bhalla, U.S. (2015). Olfactory bulb coding of odors, mixtures and sniffs is a linear sum of odor time profiles. Nature Neuroscience *18*, 272-281.

Haddad, R., Lanjuin, A., Madisen, L., Zeng, H., Murthy, V.N., and Uchida, N. (2013). Olfactory cortical neurons read out a relative time code in the olfactory bulb. Nature Neuroscience *16*, 949.

Hopfield, J.J. (1991). Olfactory computation and object perception. Proceedings of the National Academy of Sciences *88*, 6462.

Ilc, T., Werck-Reichhart, D., and Navrot, N. (2016). Meta-Analysis of the Core Aroma Components of Grape and Wine Aroma. Frontiers in Plant Science *7*, 1472.

Inagaki, S., Iwata, R., Iwamoto, M., and Imai, T. (2020). Widespread Inhibition, Antagonism, and Synergy in Mouse Olfactory Sensory Neurons In Vivo. Cell Reports *31*, 107814.

Jacob, V., Le Cam, J., Ego-Stengel, V., and Shulz, D.E. (2008). Emergent Properties of Tactile Scenes Selectively Activate Barrel Cortex Neurons. Neuron *60*, 1112-1125.

Jinks, A., and Laing, D.G. (1999). A Limit in the Processing of Components in Odour Mixtures. Perception *28*, 395-404.

Jordan, R., Fukunaga, I., Kollo, M., and Schaefer, A.T. (2018). Active Sampling State Dynamically Enhances Olfactory Bulb Odor Representation. Neuron *98*, 1214-1228.e1215.

Kato, Hiroyuki K., Chu, Monica W., Isaacson, Jeffry S., and Komiyama, T. (2012). Dynamic Sensory Representations in the Olfactory Bulb: Modulation by Wakefulness and Experience. Neuron *76*, 962-975.

Kato, Hiroyuki K., Gillet, Shea N., Peters, Andrew J., Isaacson, Jeffry S., and Komiyama, T. (2013). Parvalbumin-Expressing Interneurons Linearly Control Olfactory Bulb Output. Neuron *80*, 1218-1231.

Kay, L.M., Lowry, C.A., and Jacobs, H.A. (2003). Receptor contributions to configural and elemental odor mixture perception. Behavioral Neuroscience *117*, 1108-1114.

Koldaeva, A., Schaefer, A.T., and Fukunaga, I. (2019). Rapid task-dependent tuning of the mouse olfactory bulb. eLife *8*, e43558.

Kurahashi, T., Lowe, G., and Gold, G.H. (1994). Suppression of odorant responses by odorants in olfactory receptor cells. Science *265*, 118.

Laing, D.G., and Francis, G.W. (1989). The capacity of humans to identify odors in mixtures. Physiology & Behavior *46*, 809-814.

Laing, D.G., and Glemarec, A. (1992). Selective attention and the perceptual analysis of odor mixtures. Physiology & Behavior *52*, 1047-1053.

Laughlin, S.B. (1989). The role of sensory adaptation in the retina. Journal of Experimental Biology *146*, 39-62.

Madisen, L., Garner, Aleena R., Shimaoka, D., Chuong, Amy S., Klapoetke, Nathan C., Li, L., van der Bourg, A., Niino, Y., Egolf, L., Monetti, C.*, et al.* (2015). Transgenic Mice for Intersectional Targeting of Neural Sensors and Effectors with High Specificity and Performance. Neuron *85*, 942-958.

Malnic, B., Hirono, J., Sato, T., and Buck, L.B. (1999). Combinatorial Receptor Codes for Odors. Cell *96*, 713-723.

Marr, D. (2010). Vision: A Computational Investigation into the Human Representation and Processing of Visual Information (The MIT Press).

Mathis, A., Rokni, D., Kapoor, V., Bethge, M., and Murthy, V.N. (2016). Reading Out Olfactory Receptors: Feedforward Circuits Detect Odors in Mixtures without Demixing. Neuron *91*, 1110-1123.

Miyamichi, K., Shlomai-Fuchs, Y., Shu, M., Weissbourd, Brandon C., Luo, L., and Mizrahi, A. (2013). Dissecting Local Circuits: Parvalbumin Interneurons Underlie Broad Feedback Control of Olfactory Bulb Output. Neuron *80*, 1232-1245.

Oka, Y., Omura M Fau - Kataoka, H., Kataoka H Fau - Touhara, K., and Touhara, K. Olfactory receptor antagonism between odorants.

Penker, S., Licht, T., Hofer, K.T., and Rokni, D. (2020). Mixture Coding and Segmentation in the Anterior Piriform Cortex. Frontiers in Systems Neuroscience *14*, 89.

Poupon, D., Fernandez, P., Boisvert, S.A., Migneault-Bouchard, C., and Frasnelli, J. (2018). Can the identification of odorants within a mixture be trained? Chemical Senses *43*, 721-726.

Reddy, G., Zak, J.D., Vergassola, M., and Murthy, V.N. (2018). Antagonism in olfactory receptor neurons and its implications for the perception of odor mixtures. eLife *7*, e34958.

Rokni, D., Hemmelder, V., Kapoor, V., and Murthy, V.N. (2014). An olfactory cocktail party: figure-ground segregation of odorants in rodents. Nature Neuroscience *17*, 1225-1232.

Rokni, D., and Murthy, V.N. (2014). Analysis and Synthesis in Olfaction. ACS Chemical Neuroscience *5*, 870-872.

Shani-Narkiss, H., Vinograd, A., Landau, I.D., Tasaka, G., Yayon, N., Terletsky, S., Groysman, M., Maor, I., Sompolinsky, H., and Mizrahi, A. (2020). Young adult-born neurons improve odor coding by mitral cells. Nature Communications *11*, 5867.

Shepherd, G.M. (2004). The Synaptic Organization of the Brain, Fifth Edition edn (Oxford University Press).

Singh, V., Murphy, N.R., Balasubramanian, V., and Mainland, J.D. (2019). Competitive binding predicts nonlinear responses of olfactory receptors to complex mixtures. Proceedings of the National Academy of Sciences *116*, 9598.

Stettler, D.D., and Axel, R. (2009). Representations of Odor in the Piriform Cortex. Neuron *63*, 854-864.

Tabor, R., Yaksi, E., Weislogel, J.-M., and Friedrich, R.W. (2004). Processing of Odor Mixtures in the Zebrafish Olfactory Bulb. The Journal of Neuroscience *24*, 6611.

Verhagen, J.V., Wesson, D.W., Netoff, T.I., White, J.A., and Wachowiak, M. (2007). Sniffing controls an adaptive filter of sensory input to the olfactory bulb. Nature Neuroscience *10*, 631-639.

Wachowiak, M. (2011). All in a Sniff: Olfaction as a Model for Active Sensing. Neuron *71*, 962-973.

Wachowiak, M., and Cohen, L.B. (2001). Representation of Odorants by Receptor Neuron Input to the Mouse Olfactory Bulb. Neuron *32*, 723-735.

Weiss, T., Snitz, K., Yablonka, A., Khan, R.M., Gafsou, D., Schneidman, E., and Sobel, N. (2012). Perceptual convergence of multi-component mixtures in olfaction implies an olfactory white. Proceedings of the National Academy of Sciences *109*, 19959.

Wilson, D.A., and Stevenson, R.J. (2003). The fundamental role of memory in olfactory perception. Trends in Neurosciences *26*, 243-247.

Xu, L., Li, W., Voleti, V., Zou, D.-J., Hillman, E.M.C., and Firestein, S. (2020). Widespread receptor-driven modulation in peripheral olfactory coding. Science *368*, eaaz5390.

Zak, J.D., Reddy, G., Vergassola, M., and Murthy, V.N. (2020). Antagonistic odor interactions in olfactory sensory neurons are widespread in freely breathing mice. Nature Communications *11*, 3350.